Hindawi
Modelling and Simulation in Engineering
Volume 2024, Article ID 3767759, 15 pages
https://doi.org/10.1155/2024/3767759

Research Article

Experimental Analysis of Static and Dynamic Performance for Continuous Warren Truss Steel Railway Bridge in Heavy Haul Railway

Yiqiang Li,[1] Xianlong Luo,[2] and Yeming Li[3]

[1] *School of Safety Engineering and Emergency Management, Shijiazhuang Tiedao University, Shijiazhuang 050043, Hebei, China*
[2] *Department of Railway Engineering, Shijiazhuang Institute of Railway Technology, Shijiazhuang 050041, Hebei, China*
[3] *Tianjin Port Facilities Management Co., Ltd., 300456 Tianjin, China*

Correspondence should be addressed to Yiqiang Li; liyiq@stdu.edu.cn and Xianlong Luo; luoxianlong76@163.com

Received 16 February 2023; Revised 15 November 2023; Accepted 20 November 2023; Published 9 February 2024

Academic Editor: Marco Bonopera

Continuous Warren truss steel railway bridges are one of the main forms of railway bridges. Due to the deterioration of materials and the long-term effect of loads, the bridges will inevitably experience performance degradation, which may lead to the failure of the bridge structure to continue to operate. In order to study the mechanical properties of steel structure bridges after material deterioration and long-term loads, a continuous Warren truss steel railway bridge that has been in operation for nearly 30 years (built in 1996) is used as the research object, and a combination of field tests and finite element (FE) simulations are used to carry out research on its mechanical properties under different loads. The research results show that after nearly 30 years of operation, the steel structure bridge has local damage, but the bearing capacity still meets the requirements of heavy-duty traffic. At this stage, the corrosion of the steel structure and the damage of the bearing should be repaired in time to prevent the damage from expanding.

1. Introduction

Steel bridges have many advantages such as good long-term economy, superior mechanical properties, environmentally friendly, fast construction, and strong replaceability of components [1–3]. Therefore, the steel structure bridge is one of the bridge structures with great potential for energy saving and environmental protection. Steel structure bridges endure long-term effects of static loads such as self-weight and temperature and dynamic loads such as vehicles and wind [4–8], which will damage the structure and affect the life of the steel structure [9, 10]. Therefore, early detection of structural failure is crucial for preventing hazards and losses caused by structural failure. There are various approaches for detecting structural damage, and these approaches must be developed in large numbers for structural safety [11].

The appearance inspection and static and dynamic load tests of steel structure bridges are the keys to verifying their mechanical performance [12–15]. In addition, the test data can provide a reference for the FE simulation method of steel structure bridges and calibrate the FE simulation data [16, 17].

The experimental and simulation research of steel structure bridges is the basis of other researches on it; therefore, engineers and scholars have carried out a lot of research work on this. Wang compared the results of the static and dynamic load tests with that calculated from the FE analysis. The current conditions of the bridge are evaluated according to the codes and specifications [18]. By combining the methods of field test and FE analysis, the dynamic behaviors of the main bridge, train operation safety, and stability were researched in the article [19]. Article [20] presents a test analysis of a steel bridge's dynamic properties. The test-measured results are compared to theoretically calculated ones. Besides frequency analysis of supporting structure, the noise of the bridge during car passes is also measured and analyzed. By taking into account stress, strain, rigidity,

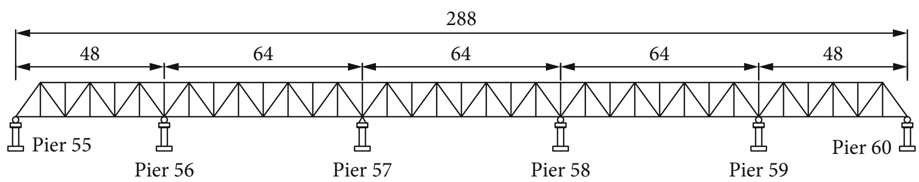

Figure 1: Span layout.

Figure 2: Real photos of the bridge structure.

natural frequency, vibration mode, damping ratio, dynamic coefficient, and dynamic parameters of amplitude, paper [21] carried out theoretical analysis and static and dynamic loading tests for structural performance evaluation. Using a numerical model combined with test data, the typical dynamic and static behaviors of a steel truss arch railway bridge are evaluated in paper [22]. Article [23] presents a structural health and performance assessment on an existing old steel pratt-typed truss railway bridge with unbraced compression chords in Malaysia using fibre optic sensors. Liu and Xiao researched the fatigue load based on the measured data [24]. El-Sisi et al. [25] performed field tests to find the actual dimension and clear cracks to validate the FE model. Through the procedure, they evaluated the bridge using AASHTO standards, Egyptian code (ECP), and S-N curves from the literature. Goto et al. [26] investigated the property of dynamic stress amplification resulting from the sudden failure of a tension member in a truss bridge by a dynamic response analysis. Vanova et al. [27] analyzed the dynamic response of a model truss bridge considering damage scenarios by vibration-based methods.

Installing appropriate static and dynamic sensors to measure the response of steel structure bridges before and after static and dynamic loading, combined with FE simulation, can effectively evaluate whether steel structure bridges have the bearing capacity specified in the specification [28], which not only ensures the operation safe of the bridge structure but also provides reference advice for the maintenance and repair of bridge structures. Therefore, relying on a continuous steel truss bridge, the mechanical characteristics of the bridge structure under static and dynamic loads are studied, the validity of the bridge condition assessment is verified, and the mechanical performance of the heavy-haul railway bridge in service is also studied. This study provides a method reference for bridge evaluation studies of the same type of bridges and provides suggestions for the maintenance and repair of heavy-duty railway steel structure bridges. The novelty of this paper is three-fold. First, provision for a feasible method for the field inspection of bridge structure and development of the detection point layout and simulation method. Second, the research method of this paper is helpful to improve the understanding of the field stress analysis of railway bridges. Third, a comparison of statical and dynamic responses at different nodal locations under different load conditions.

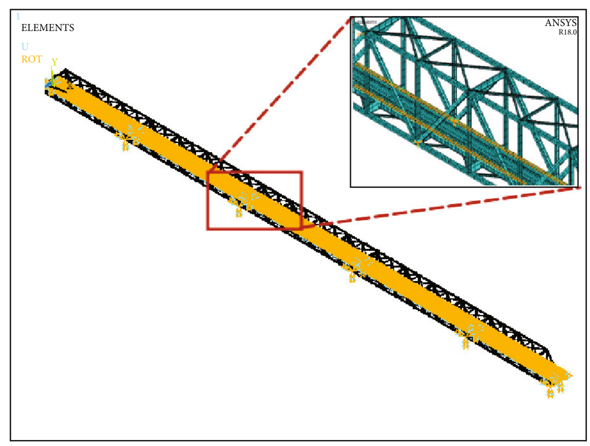

Figure 3: Finite element model of bridge structure.

2. Field Test and FE Model Introduction

2.1. Project Overview and FE Model. The bridge studied is a freight railway bridge, located in the Nanjiang Port Area of Tianjin Port. The 56th to 60th spans of the bridge to be studied are continuous Warren truss steel bridges, and the spans are arranged as $48\,\mathrm{m} + 3 \times 64\,\mathrm{m} + 48\,\mathrm{m}$. Considering the principle of structural symmetry, three spans of the steel truss bridge are selected for static and dynamic load tests. During the damage investigation, it was found that some components of the steel truss girder in the 56th to 58th

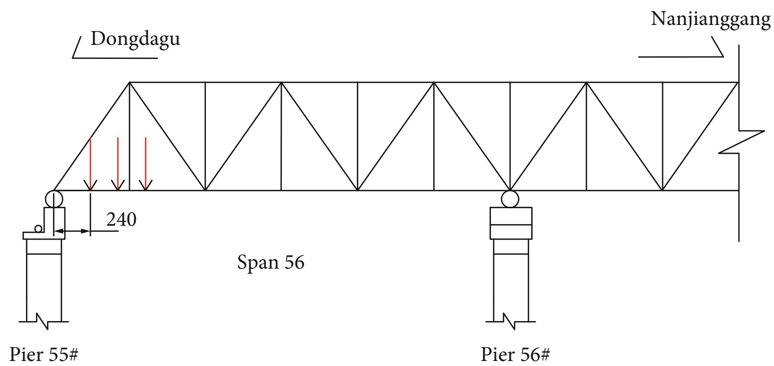

Figure 4: Loading position to maximum stringer bending moment (unit: cm).

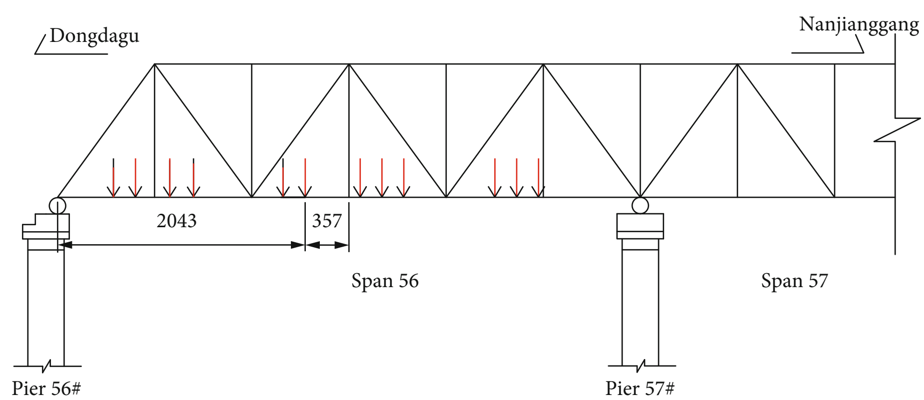

Figure 5: Loading position to maximum deflection in the 56th span and maximum stress in diagonal of the bridge gantry (unit: cm).

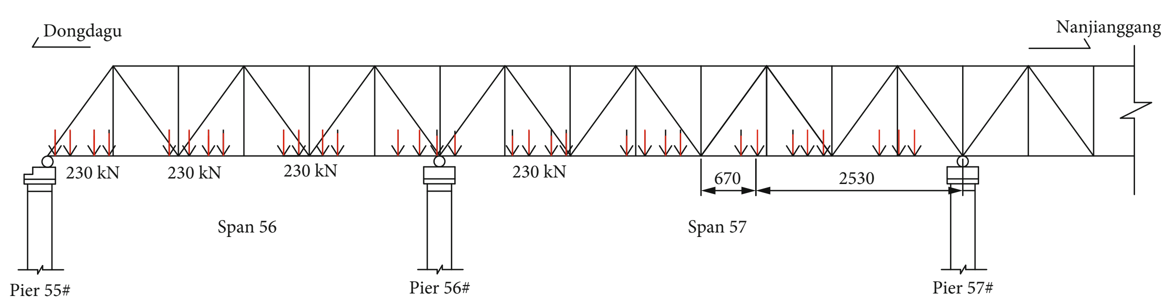

Figure 6: Loading position to maximum stress in diagonal of the 56th span (unit: cm).

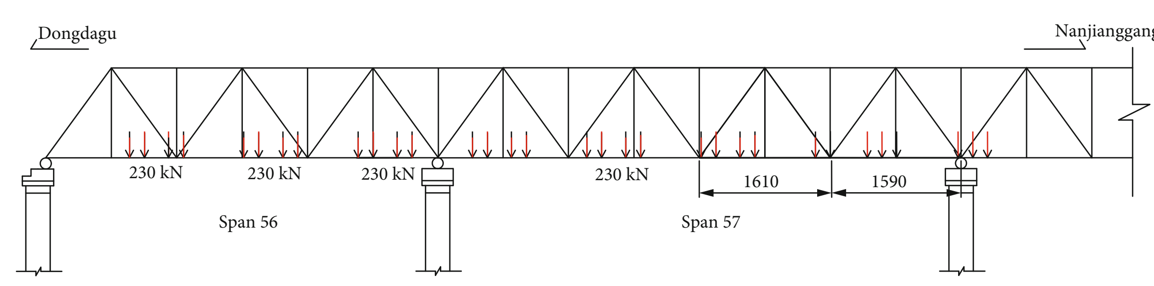

Figure 7: Loading position to maximum deflection of the 57th span and maximum negative beam bending moment at the 56# pier top (unit: cm).

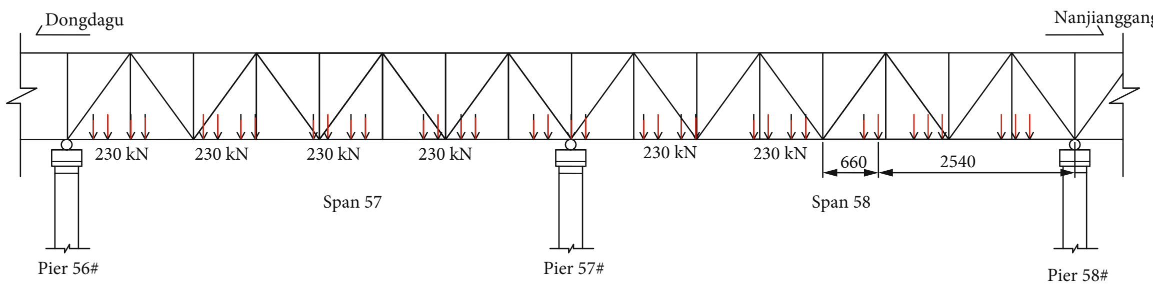

Figure 8: Loading position to maximum stress in diagonal of the 57th span (unit: cm).

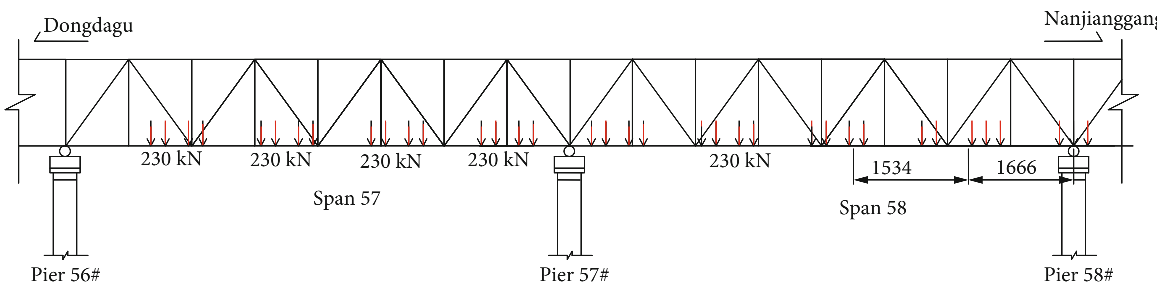

Figure 9: Loading position to maximum deflection of the 58th span and maximum negative beam bending moment at the 57# pier top (unit: cm).

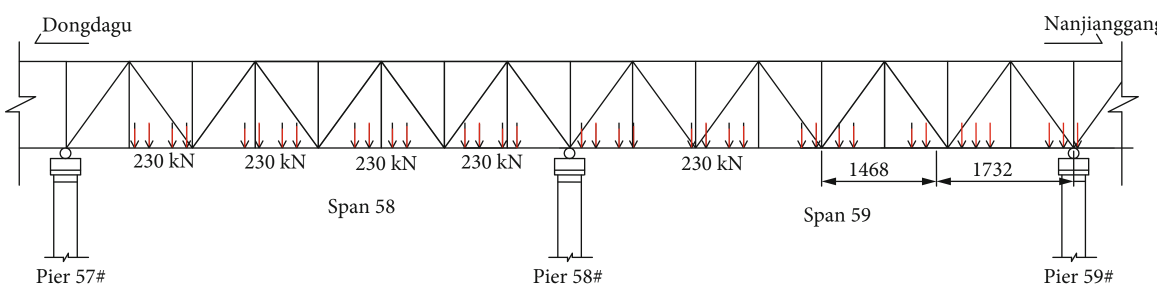

Figure 10: Loading position to maximum negative beam bending moment at the 58# pier top (unit: cm).

spans were seriously corroded. The test spans of the steel truss bridge were selected as the 56th to 58th spans. The span layout of the bridge is shown in Figures 1 and 2. The fixed supports of the continuous steel truss bridge are arranged at pier 57#, and the rest are sliding supports.

The bridge model is established by the software ANSYS, and the main truss, longitudinal and transverse beams, and connection systems are all simulated by the three-dimensional Timoshenko beam element BEAM189, as shown in Figure 3. The connections between the main truss, the beams, and the connecting system are all rigid connections. In the design, to reduce the height of the bridge building, the longitudinal and transverse beams are set at unequal heights, and the rigid beam unit MPC184 is used to simulate the rigid connection between the longitudinal beams and the transverse beams. The sleepers and rails are simulated by the three-dimensional Euler beam unit BEAM4. The steel is 16 Mnq, the elastic modulus is 2.06 $\times$ 105 MPa, the density is 7850 kg/m^3, and the Poisson's ratio is 0.3. According to the quality of the gusset plate and high-strength bolts of the continuous steel truss bridge given by the design drawings, MASS21 mass elements are used, which are evenly distributed at each node, and other auxiliary masses are evenly distributed on the vertical and horizontal beams by using MASS21 mass elements. Element COMBIN14 spring simulates the base plate between the beam and rail fastening or sleeper. Structural connections are achieved through shared nodes and rigid connections.

Figure 11: Loading test photo.

Table 1: Statistics of static loading cases for steel truss bridges.

Cases	Train loading	Case description	Cycles
Case 1	$DF12\,locomotive + 8 \times C70\,full - load\,train + 8 \times C70\,empty\,train$	Maximum longitudinal and transverse beam bending moment	3
Case 2	$DF12\,locomotive + 8 \times C70\,full - load\,train + 8 \times C70\,empty\,train$	Maximum bending moment and maximum stress in diagonal of the bridge gantry in the 56th span	3
Case 3	$DF12\,locomotive + 8 \times C70\,full - load\,train + 8 \times C70\,empty\,train$	Maximum stress in diagonal of the 56th span	3
Case 4	$DF12\,locomotive + 8 \times C70\,full - load\,train + 8 \times C70\,empty\,train$	Maximum bending moment of the 57th span and maximum negative beam bending moment at the 56# pier top	3
Case 5	$DF12\,locomotive + 8 \times C70\,full - load\,train + 8 \times C70\,empty\,train$	Maximum stress in diagonal of the 57th span	3
Case 6	$DF12\,locomotive + 8 \times C70\,full - load\,train + 8 \times C70\,empty\,train$	Maximum bending moment of the 58th span and maximum negative beam bending moment at the 57# pier top	3
Case 7	$DF12\,locomotive + 8 \times C70\,full - load\,train + 8 \times C70\,empty\,train$	Maximum negative bending moment of the 58th span	3

Table 2: Dynamic loading conditions of steel truss bridges.

Cases	Train loading	Case description	Speed	Cycles
Case 3	$DF12\,locomotive + 8 \times C70\,full - load\,train + 8 \times C70\,empty\,train$	Train passing test	5 km/h	1
Case 4	$DF12\,locomotive + 8 \times C70\,full - load\,train + 8 \times C70\,empty\,train$	Train passing test	10 km/h	4
Case 5	$DF12\,locomotive + 8 \times C70\,full - load\,train + 8 \times C70\,empty\,train$	Train passing test	20 km/h	3
Case 6	$DF12\,locomotive + 8 \times C70\,full - load\,train + 8 \times C70\,empty\,train$	Train passing test	30 km/h	3
Case 7	$DF12\,locomotive + 8 \times C70\,full - load\,train + 8 \times C70\,empty\,train$	Train passing test	40 km/h	3
Case 8	$DF12\,locomotive + 8 \times C70\,full - load\,train + 8 \times C70\,empty\,train$	Train passing test	50 km/h	3

Figure 12: Field photo of the measurement point arrangement.

2.2. Test Cases. The process of the test is as follows: Firstly, a real bridge FE model is established, in which the maximum deflection values of different bridge span positions are obtained according to the train load combination on the bridge. In this experiment, C70 and DF12 train models are used as loading loads, and the axle weight is 230 kN. Secondly, field loading is carried out according to the simulated train load position, so as to obtain the response values such as deflection and strain under load, which are the response values of static load. Finally, the vibration response of the bridge when the train passes at different speeds is carried out to obtain the frequency value.

According to the FE model, the load distribution to the maximum response is determined as the loading position of the field test. The axle weight of the test train is 230 kN. Figure 4 shows the loading position of the train when the longitudinal beam bending moment is maximum. Figure 5 shows the loading position when the deflection of the 56th span is the largest and the stress of the diagonal of the bridge gantry is the largest. Figure 6 shows the position of the 56th span when the stress in diagonal is the maximum. Figure 7 shows the loading position when the deflection of the 57th span is the largest and the negative bending moment of the 56# pier top is the largest. Figure 8 is a diagram showing the loading position of the diagonal of the 57th span when the stress is the largest. Figure 9 shows the loading position when the deflection of the 58th span is the largest and the negative bending moment of the 57# pier top is the largest. Figure 10 shows the maximum loading position of the 58# pier top with a negative bending moment. Figure 11 shows the loading test photo.

Each test case is loaded for 3 cycles. After each loading, the stress and deflection data of the bridge structure are recorded after the data is stable. Tables 1 and 2 list the specific test cases of this test.

2.3. Measuring Point Layout. The field photo of the measurement point arrangement is shown in Figure 12. The arrangement of measuring points for the static load test is shown in

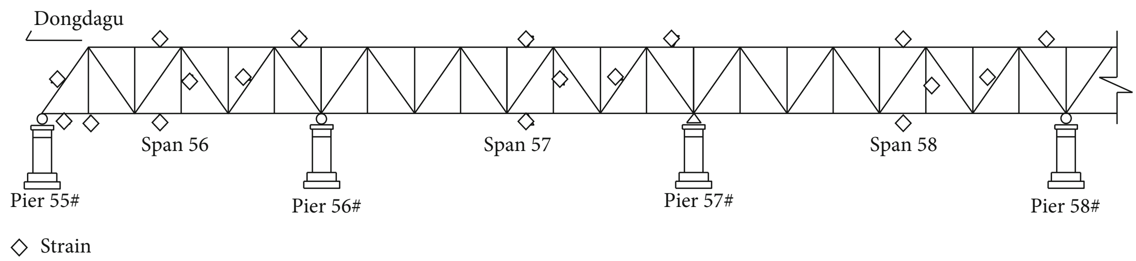

Figure 13: Longitudinal layout of strain measuring points in the static load test.

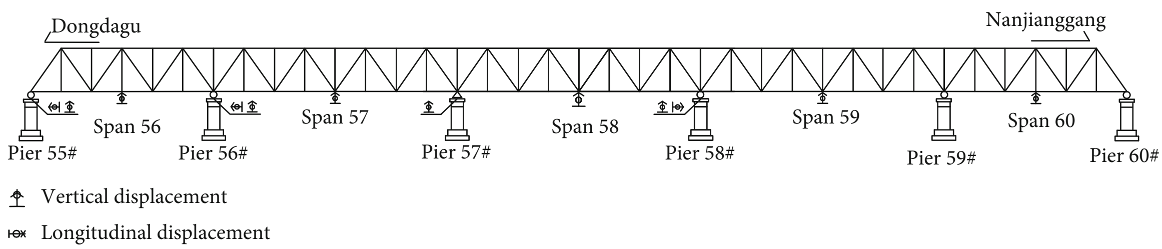

Figure 14: Longitudinal layout of static deflection measuring points.

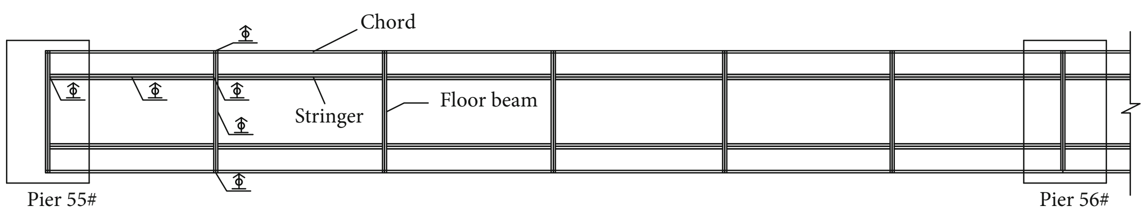

Figure 15: Longitudinal layout of deflection measuring points of stringers and floor beams.

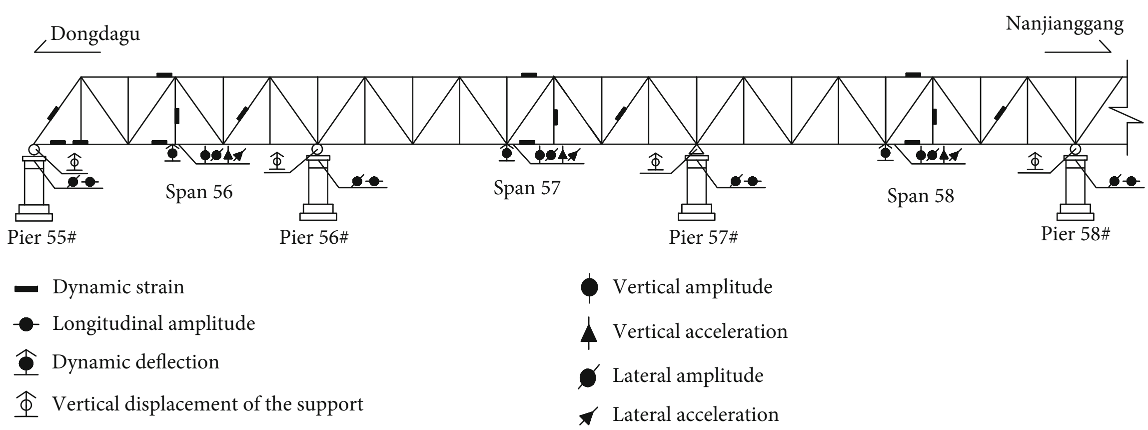

Figure 16: Longitudinal layout of dynamic measuring points.

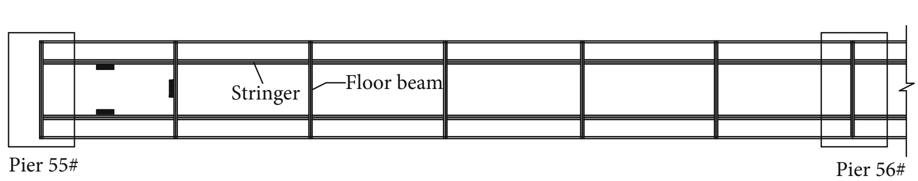

Figure 17: Longitudinal layout of dynamic strain measuring points of stringers and floor beams.

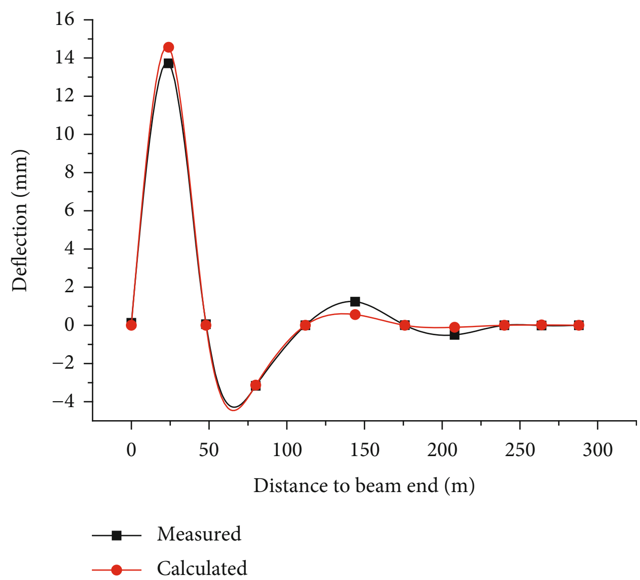

FIGURE 18: Full bridge deflection trend with loading at the span 56.

TABLE 3: Statistical table of measured stringer deflection value.

Measuring point location	Cycle 1	Cycle 2	Cycle 3	Mean	Calculated
Midspan deflection	3.38	3.26	3.31	3.32	3.81

TABLE 4: Statistical table of measured floor beam deflection value.

Measuring point location	Cycle 1	Cycle 2	Cycle 3	Mean	Calculated
Midspan deflection	1.31	1.20	1.14	1.22	1.47

Figures 13–15, and the arrangement of measuring points for the dynamic load test is shown in Figures 16 and 17.

3. Static Load Test Results and Analysis

3.1. Static Load Test Results of Span 56

3.1.1. Deflection Test Results of the Span 56. When span 56 is loaded under the maximum midspan bending moment, the measured deflection of each measuring point is shown in Figure 18, the measured deflection of the stringer is shown in Table 3, and the measured deflection of the floor beam is shown in Table 4.

3.2. The Beam Stress Test Results at the Span 56. Under the action of the test load, the comparison between the measured value and the theoretical value of the beam stress increment is shown in Table 5.

3.2.1. Analysis of the Static Load Test Results of the 56th Span

(1) Under the load of the test train, the measured average value of the midspan deflection of the 56th span is 13.72 mm, the theoretical value of deflection is 14.56 mm, and the deflection calibration coefficient is 0.94, and the deflection-span ratio converted to medium-live load is 1/2484, the deflection calibration coefficient is greater than the requirement of the normal value of [29] (0.70~0.80), and the deflection-span ratio is less than the requirement of the normal value of [29] (1/1250)

(2) Under the action of the test train load, the measured maximum value of the diagonal stress increment of the gantry of the 56th span bridge is -33.44 MPa, and the calibration coefficient is 0.89. The test coefficient is 0.85; the measured maximum value of the hip vertical stress increment is 29.67 MPa, and the verification coefficient is 0.92; the measured maximum value of the diagonal stress increment is 50.65MPa, and the verification coefficient is 0.91; the maximum stringer stress increment is 49.74 MPa, and the calibration coefficient is 0.79; the maximum floor beam stress increment is 44.91 MPa, and the calibration coefficient is 0.93. The calibration coefficients all meet the requirements of the normal values of [29]

(3) The measured maximum value of the stress increment of the midspan bottom chord is 33.96 MPa, and the calibration factor is 0.87; the calibration coefficient is greater than the requirement of the normal value of [29] (0.70~0.80)

Table 5: Stress increment at beam span 56 after loading.

Cases	Measuring point location		Stress increment value measured (MPa) Cycle 1	Cycle 2	Cycle 3	Mean	Stress increment value calculated (MPa)	Verification coefficient
Maximum stress in diagonal of the bridge gantry	Diagonal of the left bridge gantry	1#	-27.88	-27.74	-28.45	-31.83	-37.60	0.85
		2#	-30.44	-30.57	-30.68			
		3#	-37.71	-35.22	-35.98			
		4#	-32.54	-31.94	-32.78			
	Diagonal of the right bridge gantry	5#	-38.65	-38.89	-38.65	-33.44	-37.60	0.89
		6#	-27.35	-28.12	-27.99			
		7#	-27.94	-28.34	-28.74			
		8#	-38.94	-38.80	-38.82			
Maximum bending moment of span 56 midspan	Left top chord	9#	-33.62	-32.42	-33.23	-33.26	-39.17	0.85
		10#	-36.20	-34.88	-36.43			
		11#	-32.77	-32.30	-32.66			
		12#	-36.57	-37.12	-36.30			
		13#	-28.49	-27.96	-27.97			
	Left bottom chord	14#	27.79	28.47	27.67	33.96	38.95	0.87
		15#	35.38	35.53	35.26			
		16#	37.95	37.81	37.09			
		17#	28.53	28.93	28.80			
		18#	39.60	40.50	40.01			
	Right bottom chord	19#	27.30	27.68	27.43	32.98	38.95	0.85
		20#	36.38	36.53	36.26			
		21#	29.53	29.93	29.80			
		22#	33.36	33.50	33.37			
		23#	37.59	37.99	38.00			
	Left hip vertical	24#	17.96	18.35	17.23	28.56	32.12	0.89
		25#	19.01	19.01	18.87			
		26#	41.93	41.21	40.93			
		27#	39.13	38.76	38.86			
		28#	26.06	25.65	25.51			
	Right hip vertical	29#	38.57	39.34	39.36	29.67	32.12	0.92
		30#	34.71	35.37	34.99			
		31#	16.74	17.13	17.39			
		32#	17.34	17.09	16.59			
		33#	40.10	40.09	40.22			
Maximum diagonal stress of span 56	Left diagonal	34#	44.74	44.99	44.99	50.12	55.78	0.90
		35#	48.62	48.33	48.53			
		36#	55.94	56.13	56.24			
		37#	52.16	52.62	52.50			
		38#	48.74	48.61	48.73			
	Right diagonal	39#	57.52	56.95	56.80	50.65	55.78	0.91
		40#	53.11	52.57	52.56			
		41#	46.52	46.51	46.40			
		42#	47.96	47.42	47.52			
		43#	49.32	49.33	49.20			

Table 5: Continued.

Cases	Measuring point location		Stress increment value measured (MPa) Cycle 1	Cycle 2	Cycle 3	Mean	Stress increment value calculated (MPa)	Verification coefficient
Maximum negative bending moment at pier 56 top	Left top chord	44#	40.40	39.99	40.20	38.05	46.00	0.83
		45#	42.39	43.24	41.37			
		46#	38.20	35.33	36.18			
		47#	36.85	35.69	34.93			
		48#	34.66	36.21	35.15			
Maximum stress of side stringer	Left stringer	49#	-50.19	-51.07	-50.81	-49.14	-62.90	0.78
		50#	-47.00	-47.72	-48.07			
		51#	49.60	48.49	49.16	49.74	62.90	0.79
		52#	50.53	50.13	50.51			
	Right stringer	53#	-46.17	-46.99	-46.60	-43.71	-62.90	0.69
		54#	-39.19	-42.71	-40.64			
		55#	50.30	49.36	50.15	49.52	62.90	0.79
		56#	49.26	48.74	49.28			
Maximum bending moment of span 56 midspan	Side floor beam	57#	-42.23	-42.57	-42.54	-44.30	-48.52	0.91
		58#	-46.32	-46.19	-45.92			
		59#	46.25	46.14	46.89	44.91	48.52	0.93
		60#	43.88	43.01	43.27			

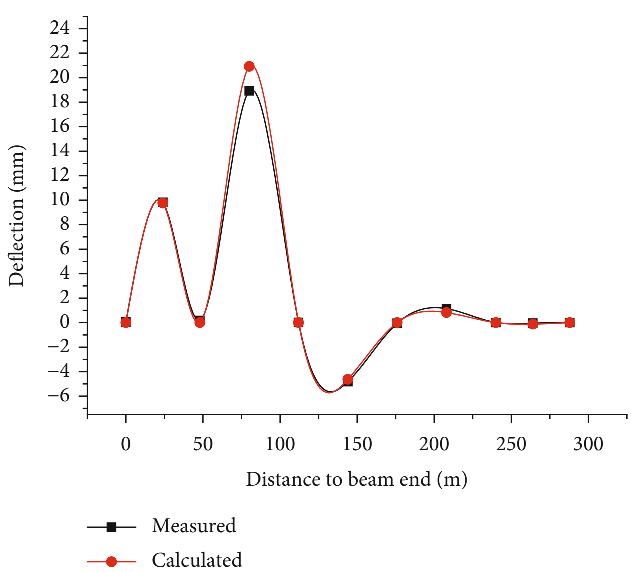

Figure 19: The deflection trend diagram of the full bridge loaded at the 57th span.

3.3. Test Results of Static Load Test of 57th Span

3.3.1. Deflection Test Results of the 57th Span. Figure 19 shows the measured deflection of each measuring point when the 57th span is loaded to the maximum midspan bending moment.

3.3.2. The Stress Test Results of the Beam Body at the 57th Span. Under the action of the test load, the comparison between the measured value and the theoretical value of the beam stress increment is shown in Table 6.

3.3.3. Analysis of the Static Load Test Results of the 57th Span

(1) Under the load of the test train, the measured average value of the midspan deflection of the 57th span is 18.92 mm, the theoretical value of deflection is 20.92 mm, the deflection calibration coefficient is 0.90, and the deflection-span ratio converted to medium-live load is 1/2131. The deflection calibration coefficient is greater than the requirement of the normal value of [29] (0.70~0.80), and the deflection-span ratio is less than the requirement of the normal value of [29] (1/1250)

(2) Under the action of the test train load, the measured maximum value of the stress increment of the upper chord in the middle span of the 57th span is -33.99 MPa, and the calibration coefficient is 0.89; the measured maximum value of the vertical stress increment is 20.34 MPa, and the calibration coefficient is 0.78; the measured maximum value of the stress increment of the diagonal is 59.84 MPa, and the calibration coefficient is 0.92. The calibration coefficients all meet the requirements of the normal value of the [29]

(3) The measured maximum value of the stress increment of the midspan and bottom chord is 30.35 MPa, and the calibration coefficient is 0.87; the calibration coefficient is greater than the requirement of the normal value of [29] (0.70~0.80)

Table 6: Stress increment after loading of the 57th span beam.

Cases	Measuring point location		Stress increment value measured (MPa)				Stress increment value calculated (MPa)	Verification coefficient
			Cycle 1	Cycle 2	Cycle 3	Mean		
Maximum bending moment of span 57 midspan	Left top chord	61#	-31.01	-31.12	-31.73	-33.99	-38.07	0.89
		62#	-35.44	-34.45	-34.16			
		63#	-36.07	-36.05	-36.01			
		64#	-33.63	-34.10	-34.19			
		65#	-33.87	-33.73	-34.23			
	Left bottom chord	66#	35.41	35.93	35.80	30.35	34.78	0.87
		67#	32.12	32.25	32.81			
		68#	28.88	29.12	29.51			
		69#	28.28	28.02	28.15			
		70#	26.55	26.14	26.28			
	Right bottom chord	71#	34.41	34.93	34.80	29.28	34.78	0.84
		72#	31.12	31.25	31.81			
		73#	25.92	25.92	25.92			
		74#	27.92	27.54	27.42			
		75#	27.23	26.18	26.89			
	Left hip vertical	76#	14.36	15.14	15.02	20.34	26.20	0.78
		77#	13.73	13.86	14.13			
		78#	31.50	31.93	32.08			
		79#	25.46	26.66	26.79			
		80#	14.89	14.89	15.13			
	Right hip vertical	81#	26.56	28.73	27.95	20.30	26.20	0.77
		82#	27.47	28.18	28.54			
		83#	14.05	13.67	14.18			
		84#	12.60	12.85	13.47			
		85#	18.41	18.66	19.17			
Maximum diagonal stress of span 57	Left diagonal	86#	54.07	54.21	54.24	59.84	65.07	0.92
		87#	57.96	57.82	57.84			
		88#	67.24	66.98	66.98			
		89#	65.35	65.35	65.25			
		90#	61.86	61.86	61.58			
	Right diagonal	91#	63.21	62.97	62.99	58.44	65.07	0.90
		92#	65.37	65.28	65.03			
		93#	53.12	53.00	52.86			
		94#	54.76	54.79	54.95			
		95#	56.31	55.89	56.01			
Maximum negative bending moment at pier 57 top	Left top chord	96#	47.01	46.45	46.29	45.44	56.17	0.81
		97#	52.58	52.97	53.12			
		98#	43.89	43.99	44.12			
		99#	43.44	43.70	43.56			
		100#	40.42	40.15	39.87			

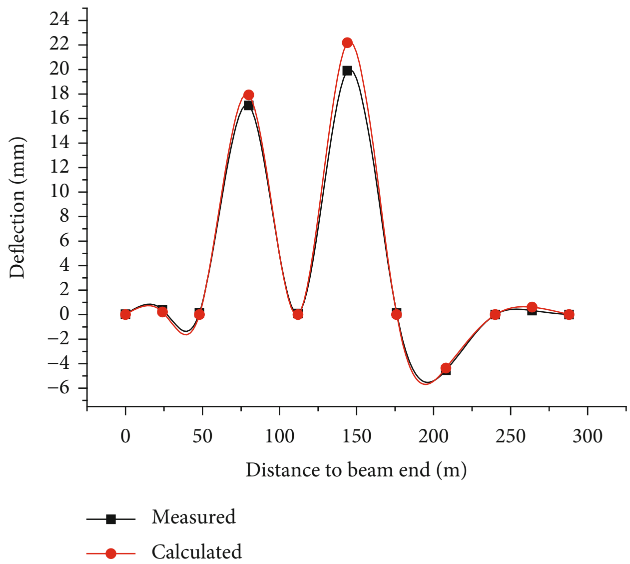

FIGURE 20: Deflection trend of the full bridge loaded at the 58th span.

3.4. Test Static Load Test Results of the 58th Span

3.4.1. Deflection Test Results of the 58th Span. When the 58th span is loaded to the maximum midspan bending moment, the measured deflection of each measuring point is shown in Figure 20.

3.4.2. The Stress Test Results of the 58th Span Beam. Under the action of the test load, the comparison between the measured value and the theoretical value of the beam stress increment is shown in Table 7.

3.4.3. Analysis of the Static Load Test Results of the 58th Span

(1) Under the action of the test train load, the average measured midspan deflection of the 58th span is 19.90 mm, the theoretical deflection value is 22.18 mm, the deflection calibration coefficient is 0.90, and the deflection-span ratio converted to medium-live load is 1/In 2026; the deflection calibration coefficient is greater than the requirement of the normal value of the [29] (0.70~0.80), and the deflection-span ratio is less than the requirement of the normal value of the [29] (1/1250)

(2) Under the load of the test train, the measured maximum value of the stress increment of the upper chord in the middle span of the 58th span is -32.70 MPa, and the calibration coefficient is 0.94; the measured maximum value of the hip vertical stress increment is 19.29 MPa, and the calibration coefficient is 0.79; the measured maximum value of the diagonal stress increment is 57.54 MPa, the calibration coefficient is 0.89, and the calibration coefficients all meet the requirements of the normal value of the [29]

(3) The measured maximum value of the stress increment of the midspan and lower chord is 28.21 MPa, and the calibration factor is 0.98; the calibration coefficient is greater than the requirement of the normal value of [29] (0.70~0.80)

4. Test Results and Analysis of Dynamic Load Test

4.1. Test Result Discussion of Dynamic Load Test of 56th Span

4.1.1. Transverse Amplitude of Bridge Span Structure. Under the action of the test train, the measured maximum transverse amplitude in the span of the 56th span bridge is 1.70 mm, which meets the requirement of 5% of the normal value (Amax) of transverse stiffness (≤3.79 mm) and the safety of transverse amplitude stipulated in the [29] limits (Amax) 5% requirement (≤6.76 mm). The results show that the stiffness of the bridge meets the requirements and the vibration under load is small.

4.1.2. Lateral Acceleration of Bridge Span Structure. Under the action of the test train, the measured maximum lateral acceleration in the span of the 56th span bridge is 0.40 m/s^2, which meets the lateral acceleration limit requirement (≤1.40 m/s^2) specified in the [29]. It shows that the transverse stiffness of the bridge is large and the antioverturning force is large.

4.1.3. Structural Dynamic Coefficient. Under the action of the test train, the maximum value of the dynamic coefficient of dynamic deflection at the midspan of the 56th span measured is 1.06, the maximum value of the dynamic coefficient of the dynamic strain of the diagonal of the bridge gantry is 1.06, and the maximum value of the dynamic coefficient of the dynamic strain of the top chord at the midspan position is 1.06. The maximum value of the dynamic strain coefficient of the chord at the lower position is 1.08, the maximum value of the dynamic strain coefficient of the vertical rod is 1.06, and the maximum value of the dynamic strain coefficient of the diagonal is 1.05, all of which meet the limit requirements of the dynamic coefficient specified in the [29] (≤1.32). It shows that the load changes little under static and dynamic action, and the load increase caused by the dynamic load effect is small.

4.1.4. Lateral Amplitude of Pier Top. Under the action of the test train, the measured maximum transverse amplitude of the pier top of the 56# pier is 0.20 mm, which meets the normal value of the transverse amplitude of the pier top (≤0.74 mm) in [29]. It indicates that the pier vibration is small.

4.2. Test Result Discussion of Dynamic Load Test of 57th Span

4.2.1. Transverse Amplitude of Bridge Span Structure. Under the action of the test train, the measured maximum transverse amplitude in the span of the 57th span bridge is 1.8 mm, which meets the requirement of 5% of the normal

Table 7: Stress increment after loading of the 58th span beam.

Case	Measuring point location		Stress increment value measured (MPa)				Stress increment value calculated (MPa)	Verification coefficient
			Cycle 1	Cycle 2	Cycle 3	Mean		
Maximum bending moment of span 58 midspan	Left top chord	101#	-37.41	-37.41	-37.64	-32.70	-34.81	0.94
		102#	-26.57	-26.43	-26.04			
		103#	-26.07	-26.18	-25.66			
		104#	-42.55	-42.01	-41.86			
		105#	-31.63	-31.49	-31.50			
	Left bottom chord	106#	30.51	30.40	30.14	28.21	28.22	0.98
		107#	25.50	25.91	25.65			
		108#	30.08	30.37	30.25			
		109#	24.55	24.41	24.27			
		110#	30.40	30.56	30.19			
	Right bottom chord	111#	26.51	26.40	26.14	27.09	28.22	0.94
		112#	25.50	25.91	25.65			
		113#	25.08	25.37	25.25			
		114#	24.45	24.99	24.58			
		115#	33.62	33.53	33.29			
	Left hip vertical	116#	12.63	13.27	13.15	18.31	24.52	0.75
		117#	12.28	12.41	12.78			
		118#	26.74	27.15	27.02			
		119#	24.50	24.65	24.52			
		120#	14.65	14.39	14.53			
	Right hip vertical	121#	23.23	23.76	23.64	19.29	24.52	0.79
		122#	25.43	26.01	25.73			
		123#	13.43	12.60	13.86			
		124#	12.96	13.74	13.75			
		125#	20.42	20.69	20.16			
Maximum diagonal stress of span 58	Left diagonal	126#	41.40	41.68	41.85	51.40	64.43	0.80
		127#	55.59	55.96	55.75			
		128#	48.70	49.34	49.51			
		129#	56.27	56.40	56.46			
		130#	54.17	53.90	54.04			
	Right diagonal	131#	61.68	61.56	61.60	57.54	64.43	0.89
		132#	63.00	63.16	63.05			
		133#	56.42	56.56	56.46			
		134#	54.32	54.61	54.51			
		135#	52.22	51.95	51.95			
Maximum negative bending moment at pier 57 top	Left top chord	136#	45.93	46.57	45.89	44.14	54.74	0.81
		137#	43.25	43.24	43.52			
		138#	41.30	41.57	41.99			
		139#	41.98	42.35	42.75			
		140#	46.93	47.36	47.52			

value of transverse stiffness (Amax) (≤5.06 mm) and the safety of transverse amplitude stipulated in [29] limits (Amax) 5% requirement (≤7.71 mm). The results show that the stiffness of the bridge meets the requirements and the vibration under load is small.

4.2.2. Lateral Acceleration of Bridge Span Structure. Under the action of the test train, the measured maximum lateral acceleration in the span of the 57th span bridge is 0.5 m/s^2, which meets the lateral acceleration limit requirements (≤1.40 m/s^2) specified in [29]. It shows that the transverse stiffness of the bridge is large and the antioverturning force is large.

4.2.3. Structural Dynamic Coefficient. Under the action of the test train, the maximum value of the dynamic coefficient of dynamic deflection at the midspan of the 57th span measured is 1.04, the maximum value of the dynamic strain coefficient of the upper chord at the midspan position is 1.08, and the maximum value of the dynamic coefficient of the dynamic strain of the lower chord at the midspan position is 1.09. The maximum value of the dynamic strain dynamic coefficient is 1.08, and the maximum value of the dynamic strain dynamic coefficient of the diagonal is 1.04, both of which meet the dynamic coefficient limit requirements (≤1.32) specified in [29]. It shows that the load changes little under static and dynamic action, and the load increase caused by the dynamic load effect is small.

4.2.4. Lateral Amplitude of Pier Top. Under the action of the test train, the measured maximum transverse amplitude of the pier top of the 57# pier is 0.2 mm, which meets the normal value of the transverse amplitude of the pier top (≤0.80 mm) in the [29]. It indicates that the pier vibration is small.

4.3. Test Result Discussion of Dynamic Load Test of 58th Span

4.3.1. Transverse Amplitude of Bridge Span Structure. Under the action of the test train, the measured maximum transverse amplitude in the span of the 58th span bridge is 1.60 mm, which meets the requirement of 5% of the normal value of transverse stiffness (Amax) (≤5.06 mm) and the safety of transverse amplitude specified in [29] limits (Amax) 5% requirement (≤7.71 mm). The results show that the stiffness of the bridge meets the requirements and the vibration under load is small.

4.3.2. Lateral Acceleration of Bridge Span Structure. Under the action of the test train, the measured maximum lateral acceleration in the span of the 58th span bridge is 0.47 m/s^2, which meets the lateral acceleration limit requirement (≤1.40 m/s^2) specified in [29]. It shows that the transverse stiffness of the bridge is large and the antioverturning force is large.

4.3.3. Structural Dynamic Coefficient. Under the action of the test train, the maximum value of the dynamic coefficient of dynamic deflection at the midspan of the 58th span measured is 1.05, the maximum value of the dynamic coefficient of the dynamic strain of the upper chord at the midspan position is 1.09, and the maximum value of the dynamic coefficient of the dynamic strain of the lower chord at the midspan position is 1.06. The maximum value of the dynamic strain dynamic coefficient is 1.03, and the maximum value of the dynamic strain dynamic coefficient of the diagonal is 1.04, both of which meet the dynamic coefficient limit requirements (≤1.32) specified in [29]. It shows that the load changes little under static and dynamic action, and the load increase caused by the dynamic load effect is small.

4.3.4. Lateral Amplitude of Pier Top. Under the action of the test train, the measured maximum transverse amplitude of the pier top of the 58# pier is 0.32 mm, which meets the normal value of the transverse amplitude of the pier top in [29] (≤0.74 mm). It indicates that the pier vibration is small.

4.3.5. Transverse Natural Vibration Frequency of Bridge Span. The measured transverse natural vibration frequency of the bridge-span structure is 2.48 Hz.

5. Conclusions

(1) Under the action of the test train load, the measured midspan deflections of the 56th to 58th spans are 13.72 mm, 18.92 mm, and 19.90 mm, respectively, and the deflection calibration coefficients are 0.94, 0.90, and 0.90, respectively, all of which do not meet the requirements of code: the normal value (0.70~0.80); the deflection-span ratios converted to medium live load are 1/2484, 1/2131, and 1/2026, which all meet the requirements of the normal value (≤1/1250)

(2) Under the load of the test train, the stress calibration coefficients of the 56th to 58th spans bridge gantry diagonals, stringer, cross beams, upper chords, vertical rods, and diagonals all meet the normal values of the code

(3) Under the load of the test train, the stress calibration coefficients of the midspan and lower chords of the 56th to 58th spans are 0.87, 0.87, and 0.98, respectively. The calibration coefficients are all larger than the requirements of the normal value (0.70~0.80), which do not meet the requirements

(4) Under the action of the test train, the vibration parameters such as the midspan lateral amplitude, midspan lateral acceleration, bridge-span lateral natural vibration frequency, dynamic deflection dynamic coefficient, and dynamic strain dynamic coefficient of the bridge spans from 56th to 58th all meet the requirements of the code

(5) Under the action of the test train, the vibration parameters such as the lateral amplitude of the pier top of the 56#~58# pier and the lateral natural vibration frequency of the bridge pier all meet the requirements of the code

(6) The two-span members and bolts of the 56th and 57th spans of the steel truss girder bridge are partially corroded. Since the bridge is located in an area with severe saline-alkali corrosion, it is recommended to remove rust and paint the corroded parts as soon as possible. The full bridge can be fully rust-proofed under certain conditions

(7) The steel truss girder bridge has the problems of missing pier inspection fences and some inspection

trolleys that cannot move. It is recommended to add pier inspection fences as soon as possible and maintain the inspection trolleys to facilitate subsequent bridge inspections and improve inspection efficiency and operation safety

Data Availability

All data, models, and codes generated or used during the study appear in the submitted article.

Conflicts of Interest

The authors declare that they have no conflicts of interest.

Acknowledgments

This work was supported by the Scientific and Technological Research Projects of Colleges and Universities in Hebei Province (CXY2023003), Key Research and Development Program of Hebei Province (19210804D), State Key Laboratory of Mechanical Behavior and System Safety of Traffic Engineering Structures (ZZ2020-19), Technology Development Project of Shuohuang Railway Development Co., Ltd (GJNY-20-230), and Science and Technology Innovation Project of China Energy Investment Corporation (SHGF-15-41).

References

[1] M. G. Barker and S. D. Schrage, “High-performance steel bridge design and cost comparisons,” *Transportation Research Record*, vol. 1740, no. 1, pp. 33–39, 2000.

[2] J. L. Durkee, *Steel Bridge Construction*, CRC Press, 2014.

[3] S. A. Kosenko, I. S. Bondar, M. Y. Kvashnin, and G. I. Chekmareva, “Ensuring the passage of freight trains with increased axle loads on railway bridges,” *Transportation Research Procedia*, vol. 61, pp. 627–635, 2022.

[4] C. W. Roeder, K. E. Barth, and A. Bergman, “Effect of live-load deflections on steel bridge performance,” *Journal of Bridge Engineering*, vol. 9, no. 3, pp. 259–267, 2004.

[5] N. Lu, L. Yang, and D. Yang, “Fatigue reliability evaluation of orthotropic steel bridge decks based on site-specific weigh-in-motion measurements,” *International Journal of Steel Structures*, vol. 19, pp. 181–192, 2018.

[6] H. Li and W. Gang, “Fatigue evaluation of steel bridge details integrating multi-scale dynamic analysis of coupled train-track-bridge system and fracture mechanics,” *Applied Sciences*, vol. 10, no. 9, p. 3261, 2020.

[7] R. Chmielewski and P. Muzolf, “Analysis of degradation process of a railway steel bridge in the final period of its operation,” *Structure and Infrastructure Engineering*, vol. 19, no. 4, pp. 537–553, 2023.

[8] E. Erduran, S. Gonen, and A. Alkanany, “Parametric analysis of the dynamic response of railway bridges due to vibrations induced by heavy-haul trains,” *Structure and Infrastructure Engineering*, vol. 20, no. 3, pp. 1–14, 2022.

[9] M. R. Saberi, A. Rahai, M. Sanayei, and R. M. Vogel, “Steel bridge service life prediction using bootstrap method,” *International Journal of Civil Engineering*, vol. 15, no. 1, pp. 51–61, 2017.

[10] M. Q. Tran, H. S. Sousa, T. V. Ngo et al., “Structural assessment based on vibration measurement test combined with an artificial neural network for the steel truss bridge,” *Applied Sciences*, vol. 13, no. 13, p. 7484, 2023.

[11] V. Patil and D. Ahiwale, “Damage detection of Warren truss bridge using frequency change correlation,” *Materials Today: Proceedings*, vol. 56, pp. 18–28, 2022.

[12] P. Tomáš, P. Michal, and R. Pavel, “Assessment of an Old Steel Railway Bridge Using Dynamic Tests,” in *X International Conference on Structural Dynamics, EURODYN 2017*, pp. 3053–3053, 2017.

[13] J. Häggström, T. Blanksvärd, P. Collin, and T. Yongming, “Full-scale testing to failure of a steel truss railway bridge,” *Proceedings of the Institution of Civil Engineers-Bridge Engineering*, vol. 170, no. 2, pp. 93–101, 2017.

[14] P. A. Montenegro, H. Carvalho, D. Ribeiro et al., “Assessment of train running safety on bridges: a literature review,” *Engineering Structures*, vol. 241, article 112425, 2021.

[15] M. Bonopera, K. C. Chang, C. C. Chen, T. K. Lin, and N. Tullini, “Bending tests for the structural safety assessment of space truss members,” *International Journal of Space Structures*, vol. 33, no. 3-4, pp. 138–149, 2018.

[16] Y. Shi-ruo, C. H. Dan-qing, and C. Qing-yuan, “Simulation vibration analysis of train and railway continuous steel truss bridge,” *Journal of Beijing University of Technology*, vol. 39, no. 3, pp. 385–388, 2018.

[17] R. D. Shibeshi, *Dynamic Analysis of Steel Railway Bridge Subjected to Train Loads*, University of Pretoria, 2016.

[18] Z. H. Ping-wei, S. H. Gang, Q. Jin-huan, and W. Shuang-yan, “Load test study of Changshou Changjiang River Bridge on Chongqing-Huaihua Railway,” *Bridge Construction*, vol. 1, pp. 134–137, 2006.

[19] Y. Jing-chuan, Y. Jing, W. Wei, Y. Yi-qian, K. Zai-tian, and L. Penghui, “Research on the dynamic performances of the steel truss girder main bridge of Jinan Yellow River extra large bridge for high-speed railway,” *China Railway Science*, vol. 34, no. 3, pp. 7–13, 2013.

[20] R. Fojtík, T. Novotný, I. Skotnicová, M. Stolárik, N. Zdražilová, and M. Pinka, “Dynamic experimental analysis of a steel bridge,” *Advanced Materials Research*, vol. 1020, pp. 215–220, 2014.

[21] Y. Yang and Q. C. Shen, “Static and dynamic loading tests and structural analysis for Rongjiang River Bridge with continuous steel truss and flexible arch in Xiamen-Shenzhen Railway,” *Journal of Railway Science and Engineering*, vol. 11, no. 4, pp. 19–25, 2014.

[22] Y. S. Song, Y. L. Ding, H. W. Zhao, G. X. Wang, A. Q. Li, and B. Y. Cao, “Structural behavior analysis of a continuous steel truss arch railway bridge integrating monitoring data,” *Advances in Mechanical Engineering*, vol. 9, no. 1, Article ID 1687814016683316, 2016.

[23] S. C. Lee, B. P. Tee, M. F. Chong, K. M. Ku Mahamud, and H. Mohamad, “Structural assessment for an old steel railway bridge under static and dynamic loads using fibre optic sensors,” in *International Conference on Smart Infrastructure and Construction 2019 (ICSIC)*, Churchill College, Cambridge, 2019.

[24] X. Liu and X. Xiao, “Study of a railway steel bridge train load model based on measured data,” in *IABSE Conference, Seoul 2020: Risk Intelligence of Infrastructures*, pp. 42–50, Seoul, South Korea, November 2020.

[25] A. E. El-Sisi, O. M. El-Husseiny, E. B. Matar, H. E. Sallam, and H. A. Salim, "Field-testing and numerical simulation of vantage steel bridge," *Journal of Civil Structural Health Monitoring*, vol. 10, no. 3, pp. 443–456, 2020.

[26] G. Yoshiaki, K. Naoki, and H. Issei, "Dynamic stress amplification caused by sudden failure of tension members in steel truss bridges," *Journal of Structural Engineering*, vol. 137, no. 8, pp. 850–861, 2011.

[27] P. Vanova, Z. Sun, O. E. Odinson, and Z. Jiang, "Dynamic response analysis of a model truss bridge considering damage scenarios," *Engineering Failure Analysis*, vol. 151, article 107389, 2023.

[28] R. Silva, D. Ribeiro, C. Costa, A. Arêde, and R. Calçada, "Experimental validation of a non-linear train-track-bridge dynamic model of a stone arch railway bridge under freight traffic," *International Journal of Rail Transportation*, vol. 12, no. 4, pp. 1–32, 2022.

[29] Ministry of Railways of the People's Republic of China, *Code for Rating Existing Railway Bridge*, China Railway Publishing House, Beijing, China, 2004.